Imaging of the Glucagon Receptor in Subjects with Type 2 Diabetes

Olof Eriksson[1,2], Irina Velikyan[3,4], Torsten Haack[5], Martin Bossart[5], Iina Laitinen[6], Philip J. Larsen[5], Jan Erik Berglund[7], Gunnar Antoni[3,4], Lars Johansson[1], Stefan Pierrou[1], Joachim Tillner[8], and Michael Wagner[5]

[1]Antaros Medical AB, Uppsala, Sweden; [2]Science for Life Laboratory, Department of Medicinal Chemistry, Uppsala University, Uppsala, Sweden; [3]Department of Medicinal Chemistry, Uppsala University, Uppsala, Sweden; [4]Akademiska Sjukhuset, Uppsala, Sweden; [5]R&D Research Platform, Integrated Drug Discovery, Sanofi, Frankfurt, Germany; [6]Global Imaging, Sanofi, Frankfurt, Germany; [7]Clinical Trial Consultants AB, Uppsala, Sweden; and [8]Translational Medicine, Sanofi, Frankfurt, Germany

Despite the importance of the glucagon receptor (GCGR) in disease and in pharmaceutical drug development, there is a lack of specific and sensitive biomarkers of its activation in humans. The PET radioligand ^{68}Ga-DO3A-VS-Tuna-2 (^{68}Ga-Tuna-2) was developed to yield a noninvasive imaging marker for GCGR target distribution and drug target engagement in humans. **Methods:** The biodistribution and dosimetry of ^{68}Ga-Tuna-2 was assessed by PET/CT in 13 individuals with type 2 diabetes as part of a clinical study assessing the occupancy of the dual GCGR/glucagon like peptide-1 receptor agonist SAR425899. Binding of ^{68}Ga-Tuna-2 in liver and reference tissues was evaluated and correlated to biometrics (e.g., weight or body mass index) or other biomarkers (e.g., plasma glucagon levels). **Results:** ^{68}Ga-Tuna-2 binding was seen primarily in the liver, which is in line with the strong expression of GCGR on hepatocytes. The kidneys demonstrated high excretion-related retention, whereas all other tissue demonstrated rapid washout. The $SUV_{55\ min}$ (SUV during the last 10-min time frame, 50–60 min after administration) uptake endpoint was sensitive to endogenous levels of glucagon. ^{68}Ga-Tuna-2 exhibited a safe dosimetry profile and no adverse events after intravenous administration. **Conclusion:** ^{68}Ga-Tuna-2 can be used for safe and accurate assessment of the GCGR in human. It may serve as an important tool in understanding the in vivo pharmacology of novel drugs engaging the GCGR.

Key Words: glucagon; PET; metabolic disease; obesity; type 2 diabetes

Glucagon is a crucial hormone in energy metabolism. It is secreted by the pancreatic α-cells in response to decreased glucose availability in the bloodstream. Glucagon exerts both autocrine (inhibition feedback), paracrine (on other islet cell subtypes including β-cells), and endocrine effects via activation of the glucagon receptor (GCGR). Its main endocrine action occurs in hepatocytes in the liver, where GCGR activation triggers breakdown of glycogen and subsequent release of glucose to the bloodstream. Glucagon is a life-saving hormone to reverse hypoglycemia (1).

Glucagon signaling has furthermore been associated to increased energy expenditure. The GCGR has therefore recently come into focus also as a pharmaceutical target, especially in the context of bi- or trimodal peptide agonists for the treatment of metabolic disease and obesity (2–4). These usually combine GCGR agonism with agonism of one or both of the incretin hormone receptors: the glucagon like peptide-1 receptor (GLP1R) and the gastric inhibitory peptide receptor.

Despite the importance of the GCGR in disease and in pharmaceutical drug development, there is a lack of specific and sensitive biomarkers of its activation in human physiology. Furthermore, some physiologic effects of GCGR activation (inhibition of food intake, glucose homeostasis) tend to overlap with that of the incretins, making it difficult to disentangle GCGR target engagement and occupancy for the new class of polyagonists. On the basis of this need, we recently developed the PET ligand ^{68}Ga-DO3A-VS-Tuna-2 (^{68}Ga-Tuna-2). ^{68}Ga-Tuna-2 (also known as ^{68}Ga-DO3A-GCG-S01) binds to the GCGR in the liver with high specificity and affinity both in vitro and in vivo in several species including rat and nonhuman primate (NHP) (5,6).

The dual glucagon like peptide-1 receptor (GLP1R)/GCGR agonist SAR425899 demonstrated promising effects on weight loss and glucose control in preclinical and clinical studies (7–10). A clinical PET imaging study was therefore performed with the objective of evaluating the respective receptor occupancy of the dual agonist SAR425899 in individuals with type 2 diabetes (T2D) (ClinicalTrials.gov: NCT03350191). Occupancy of the GCGR in the liver and GLP1R in the pancreas was determined by baseline and on-drug PET/CT examinations using ^{68}Ga-Tuna-2 and ^{68}Ga-DO3A-VS-Exendin4, respectively. The details of the clinical SAR425899 occupancy study were reported separately (11).

Here, we report the first-in-human results of the biodistribution, liver binding, and dosimetry of ^{68}Ga-Tuna-2, based on the baseline examination of 13 individuals with T2D.

MATERIALS AND METHODS

Study Population

The baseline ^{68}Ga-Tuna-2 examinations were performed as a part of a phase Ib, single-center, open-label study assessing the GCGR and GLP1R occupancy of SAR425899 in overweight to obese T2D patients (ClinicalTrials.gov: NCT03350191). Individuals with a diagnosis of T2D for at least 1 y at the time of inclusion participated in the study (male

or female, 18–75 y old). T2D-related comorbidities were allowed. Otherwise, the individuals were generally healthy with normal vital signs as assessed by the investigator. Exclusion criteria included any medication except for stable metformin treatment, sulphonylureas or medication for allowed comorbidities, pregnancy or breastfeeding. In total, 13 individuals with T2D underwent the ^{68}Ga-Tuna-2 baseline PET examinations, which are reported here. Body weight and fasting plasma glucose were measured at baseline and before breakfast and dosing at the end of treatment. The study was approved by the Swedish Ethical Review Authority. All subjects signed a written informed consent form. Study protocols were approved by the Swedish Medical Product Agency, and the trial was performed in accordance with the guidelines established by the Declaration of Helsinki and the International Conference on Harmonization—Good Clinical Practice.

Radiochemistry

Good-manufacturing-practice grade DO3A-VS-Tuna-2 was provided by Sanofi. The good-manufacturing-practice–compliant production of ^{68}Ga-Tuna-2 was developed and conducted on an automated synthesizer (Modular Lab Pharm Tracer; Eckert & Ziegler) using a disposable cassette system. The synthesis of ^{68}Ga-Tuna-2 for clinical studies was recently described in detail (12) and was developed based on, respectively, a manual radiolabeling procedure (5) and an automated procedure (13) developed earlier for similar peptide ^{68}Ga-DO3A-VS-Exendin4. The product formulated in saline containing ethanol (<10%) was supplied in a sterile glass vial. The radiochemical yield was over 90% with no unknown single impurity of over 5%.

PET/CT Examination

Each individual was given standardized meals on the evening before, for breakfast, and lunch leading up to the PET scans to minimize variability in, for example, plasma glucagon levels. The lunch (lasagna) was administered 3 h before the PET/CT examination, and the participants were otherwise fasting. Venous blood samples were collected just before the PET/CT examination for assessment of levels of endogenous glucagon. Blood was collected in P800 tubes (BD) to prevent proteolytic degradation, and glucagon was analyzed using the Mercodia ELISA assay. Blood glucose was also assessed 5, 30, and 60 min after administration of PET radiopharmaceutical. The individuals were positioned with assistance of a CT scout (lateral, 120 kV, 10 mAs) to include the liver in the 20 cm field of view of a Discovery MI PET/CT scanner (GE Healthcare). Attenuation correction and anatomic coregistration were provided by a CT examination (120 kV, Auto mA 10–30 mAs, noise-index 170, rotation time 0.5 s, full spiral, slice thickness 3.75 mm, pitch 1.53:1).

Then, a target dose of ^{68}Ga-Tuna-2 (0.5 MBq/kg) was administered intravenously (0.46 ± 0.031 MBq/kg, corresponding to 0.13 ± 0.068 µg/kg DO3A-VS-Tuna-2 peptide mass). Dynamic PET measurements were acquired over 60 min and reconstructed by an iterative VPFX-S algorithm (3 iterations, 3 subsets, matrix 256 × 256, z-axis postprocessing filter 3 mm) with all relevant corrections performed (30 frames in total: 12 × 10 s, 6 × 30 s, 5 × 120 s, 5 × 300 s, 2 × 600 s).

For 3 individuals, arterial sampling was performed 5, 30 and 60 min after ^{68}Ga-Tuna-2 administration to measure the radioactivity in whole blood and plasma (to calculate the plasma–to–whole-blood concentration ratios) as well as to determine the metabolic stability of ^{68}Ga-Tuna-2 in humans.

Since this was a first-in-human study, each patient underwent additional monitoring before, during, and after the administration of ^{68}Ga-Tuna-2 according to the local hospital safety routines. The monitoring included inspection of injection site, and logging of blood pressure, 12-lead electrocardiogram, heart rate and general appearance throughout the imaging examination. A follow-up electrocardiogram and inquiry on perceived adverse events are performed in person or over the phone 24 h after the examination.

Metabolic Stability

Blood samples were centrifuged at 4,000 rpm for 2 min at 4°C (Beckman Allegra X-22R Centrifuge). From the plasma, 0.5 mL was taken, and an equal volume of acetonitrile was added to precipitate the proteins. The mixture was centrifuged at 13,200 rpm at 4°C for 1 min (Eppendorf 5415R centrifuge; Eppendorf AG). The supernatant was filtered through a 0.2-µm nylon membrane (Corning Inc.) by centrifugation at 13,200 rpm at 4°C for 1 min. The filtered supernatant (500 µL) was diluted with 1,500 µL H2O, and then 30 µL 0.01 mM of unlabeled DO3A-VS-Tuna-2 peptide were added to the mixture. The sample preparation recovery was determined by measuring the radioactivity in the plasma, filters, and pellet.

High-performance liquid chromatography analysis was performed using a binary pump system (Gilson). The sample (1.8 mL) was injected using an automated solid-phase extraction controller (ASPEC; Gilson) connected to a dilutor (Gilson). The separation was performed on an Xbridge Prep BEH130 C18 (peptide separation technology, 250 × 10 mm, inner diameter 5 µm with a 10 × 10 mm C18 security guard) from the same supplier. The high-performance liquid chromatography system was operated at a flow rate of 6 mL/min. The mobile phase consisted of 0.1% trifluoroacetic acid in MilliQ:0.1% trifluoroacetic acid in acetonitrile. Gradient elution mode was used for the separation (gradient: 0–7 min: 5%–70%, 7–12 min: 70%, 12–13 min: 70%–5%, 13–15 min: 5%)

A second method was developed with a lesser gradient, to determine whether any metabolites were coeluting with the DO3A-VS-Tuna-2 peak. An ultraviolet detector (Gilson) was used to detect unlabeled DO3A-VS-Tuna-2 at 220 nm. The outlet from the detector was connected to a switching valve on the arm of the ASPEC to enable automatic fraction collection. Six fractions were collected, and the radioactivity in the fractions was measured by a well-type scintillation counter. A radio detector (Radiomatic 610TR) was coupled in series with the ultraviolet detector.

PET Image Analysis

Tissues of interest (liver, kidney, spleen, and erector spinae muscle) were segmented on coregistered PET/CT images normalized to display the SUV (i.e., corrected for administered dose in MBq and body weight) in each voxel (Carimas software, version 2.9; Turku PET Center). The full organ volume was segmented if inside the field of view. The liver segmentation was further divided into to the left and right part of the liver, approximately divided by a hypothetical diagonal line from the gallbladder to the vena cava (i.e., Cantlie's line). The aorta was delineated by segmenting single voxels fully within the lumen of aorta descendant as identified on early PET frames and coregistered CT projections.

Human Predicted Dosimetry

The dosimetry of ^{68}Ga-Tuna-2 was estimated based on the dynamic biodistribution in the human abdomen. Briefly, the SUVs in each tissue at several time points (5, 10, 20, 30, 40, 50, and 60 min) were normalized to that of a human adult whole-body reference phantom. In tissues in which human biodistribution was not available (due to the limited field of view of the scanner), data from NHPs were imputed. The decay-corrected and normalized SUVs were back-corrected to count rates to calculate the actual radiation burden in each tissue. The tissue residence times (MBq*h/MBq) were assessed by trapezoidal approximation of the back-corrected biodistribution data. The residence time from the last measured time point (60 min) until infinity in each tissue was estimated as monoexponential decay of the nuclide (assuming negligible washout).

The absorbed dose in an adult reference male phantom (ICRP60) was calculated from the residence time in each tissue (OLINDA/EXM 1.1 software; Vanderbilt University). The organ-specific doses are reported as mGy/MBq (effective dose as mSv/MBq). The amount of MBq that can be safely administered annually (MBq/y) was calculated for each organ as well as the effective dose, by dividing the limiting dose (10 mSv/y for the effective dose, 150 mGy/y for all tissues except for red marrow with 50 mGy/y) by the absorbed dose per MBq (mGy/MBq or mSv/MBq). Extrapolation of human dosimetry was previously performed based on rat (5) and NHP (6) biodistribution in a similar manner; these are included here for comparison.

Statistics

Data on the group level are reported as mean $\pm$ SD. Statistical analysis was performed in GraphPad Prism 6.0 (GraphPad Software), and differences between groups were assessed by the Student t test using a significance level of $P < 0.05$.

RESULTS

Patient Population

The age of the patient population ($n = 13$) was 65.9 ± 8.8 y (range, 49–75 y). The body weight was 97.77 ± 8.09 kg (range, 79–111 kg), and the body mass index was 31.38 ± 2.96 kg/m^2 (range, 27.76–37.20 kg/m^2). Most patients were male (12 [92.3%] of 13 patients).

No adverse events occurred during the ^{68}Ga-Tuna-2 PET scans, and all ($n = 13$) baseline examinations were performed in their entirety as planned.

The results of the occupancy of SAR425899 are reported separately (12). Briefly, SAR425899 demonstrated stronger activity on the GLP1R in the pancreas (on average 48% occupancy) than on the GCGR in the liver (on average 11% occupancy), which was in line with the in vitro potency on the respective receptor.
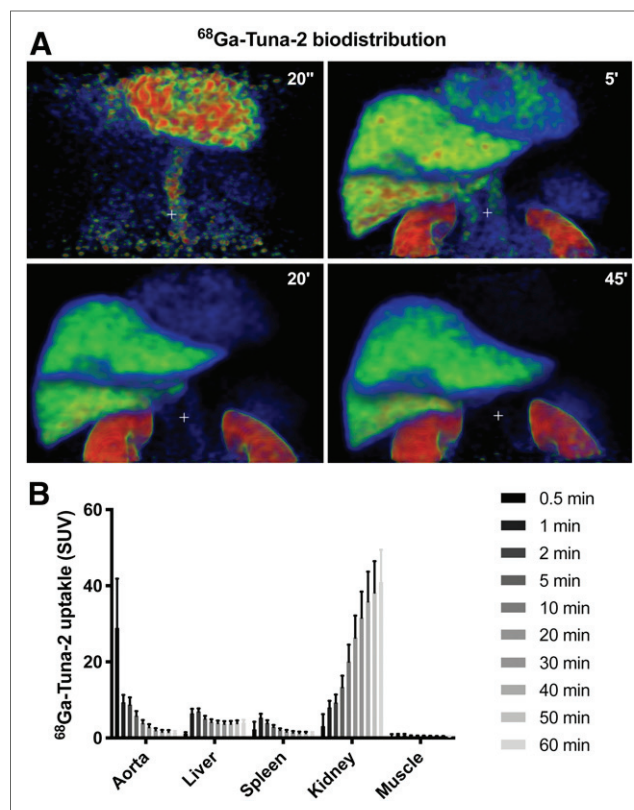
Biodistribution of ^{68}Ga-Tuna-2

On a group level, ^{68}Ga-Tuna-2 rapidly accumulated in the blood pool (Figs. 1A, top left panel, and 1B), followed by extraction into the liver and kidney and to a lesser extent tissues such as the spleen (Fig. 1A, top right panel). Uptake in the spleen and blood pool was progressively cleared during the examination (Fig. 1A, bottom left and right panels), whereas retention was seen in the liver and kidney. The biodistribution on group levels is summarized in Figure 1B.

The dynamic analysis showed that the hepatic uptake displayed strong retention over 60 min in all individuals (Fig. 2A). The spleen exhibited early tracer delivery similar to the liver but then demonstrated rapid washout of tracer (Fig. 2B). The aorta similarly displayed fast clearance in all individuals (Fig. 2C). The SUV during the last 10-min time frame, 50–60 min after administration (i.e., SUV$_{55\ min}$), provided the optimal image contrast for GCGR-positive liver tissue compared with GCGR-negative spleen and aorta, and was therefore used as surrogate endpoint for GCGR density.

^{68}Ga-Tuna-2 uptake in the liver was high (liver SUV$_{55\ min}$ = 3.96 ± 0.80) at the end of the examination, indicating high density of glucagon receptors (Fig. 2D). The amplitude of the hepatic binding was significant in comparison with GCGR-negative spleen (splenic SUV$_{55\ min}$ = 1.21 ± 0.38, $P < 0.0001$) and the aortic blood pool (aortic SUV$_{55\ min}$ = 1.40 ± 0.42, $P < 0.0001$). The spleen exhibited uptake similar to or lower than the blood pool, indicating negligible binding of ^{68}Ga-Tuna-2.

Arterial blood samples were acquired after ^{68}Ga-Tuna-2 administration, for measurement of radioactivity in plasma and whole

FIGURE 1. (A) Representative 3-dimensional projection of biodistribution in abdominal region as assessed by PET at 20 s, 5 min, 20 min, and 45 min after administration of ^{68}Ga-Tuna-2. (B) Average biodistribution ($n = 13$ subjects diagnosed with T2D) of ^{68}Ga-Tuna-2 in abdominal tissues.

blood as well as the metabolic stability of the radiolabeled peptide in plasma. The rate of metabolic degradation of ^{68}Ga-Tuna-2 in arterial plasma was relatively slow, with approximately 85% intact tracer after 60 min (Table 1). The plasma–to–blood-partition ratio was estimated to be constant throughout the examination (approximately 1.9).

GCGR Density in Different Liver Parts

There was a distinct difference in uptake of ^{68}Ga-Tuna-2 between the right and left parts of the liver, indicating a heterogeneous distribution of the GCGR in liver (Figs. 3A–3C). The binding in the left part was on average $20.5\% \pm 8.7\%$ (range, 6.2–39.0) lower than in the right part. A decrease was seen in all individuals but was also apparent on a group level. The difference was increasingly seen from 1 min and forward, but not during the initial biodistribution/perfusion phase (<30 s), where uptake in the left part in fact was higher (Fig. 3D).

Sensitivity to Levels of Coadministered DO3A-VS-Tuna-2 Peptide and Endogenous Glucagon

Liver uptake measured as SUV$_{55\ min}$ at the baseline examination correlated to the levels of glucagon in plasma ($R^2 = 0.33$, $P < 0.05$) (Fig. 4A). This is expected to some degree, as ^{68}Ga-Tuna-2 engages the same binding site as endogenous glucagon. Thus, if the baseline value is to be compared with an assessment in which the subject exhibited lower or higher endogenous plasma glucagon levels, a correction should be performed.
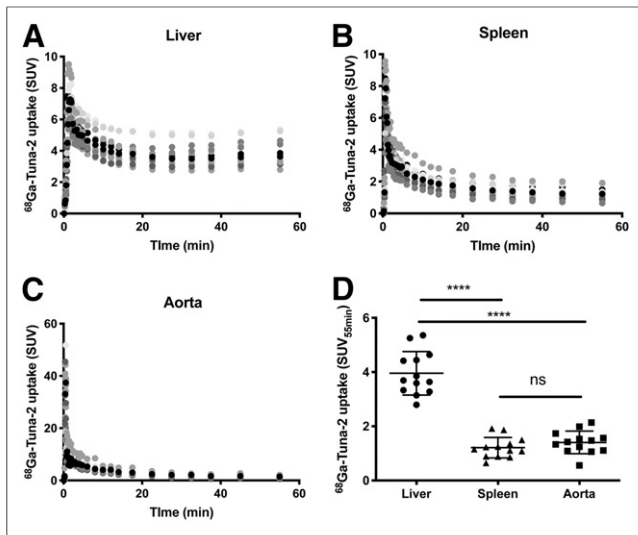
FIGURE 2. Dynamic uptake of ^{68}Ga-Tuna-2 in GCGR rich liver (A), GCGR-negative spleen (B), and aorta (C) over 60 min. (D) Comparison of uptake in tissues at 55-min time point (SUV$_{55\ min}$, 50–60 min after administration).

There was no mass effect (i.e., significant blocking effect of the amount of unlabeled DO3A-VS-Tuna-2 peptide coadministered with the tracer dose) in liver uptake expressed as SUV$_{55\ min}$ due to the peptide mass dosages given at the baseline examination (Fig. 4B). This is in line with the dose escalation data in NHPs, where negligible mass effect was observed as peptide doses $< 0.2\ \mu g/kg$ DO3A-VS-Tuna-2.

Correlations to Physiologic Factors

GCGR density in the liver did not correlate with factors such as weight ($R^2 = 0.16$, $P = 0.18$), body mass index ($R^2 = 0.02$, $P = 0.64$), or age ($R^2 = 0.12$, $P = 0.25$).

However, GCGR density correlated inversely with liver volume ($R^2 = 0.55$, $P < 0.01$) (Fig. 4C), that is, in individuals with a large liver the density of GCGR is low.

Although anecdotal, the only female (1/13) enrolled in the study exhibited the higher GCGR density in the liver (SUV$_{55\ min}$ = 5.4). The same individual additionally had among the lower GCGR heterogeneity between the right and left liver parts.

Human Predicted Dosimetry

Human predicted dosimetry of ^{68}Ga-Tuna-2 was based on human, NHP, and rat biodistribution data (Fig. 5A), and the regulatory acceptable amounts of MBq of ^{68}Ga-Tuna-2 that can be

TABLE 1
Metabolic Stability and Blood Plasma Partition of ^{68}Ga-Tuna-2 in Humans ($n = 3$)

Time (min)	Intact peptide (%)	Plasma-to-blood ratio (1/1)
5	97.8 ± 0.6	1.85 ± 0.04
30	92.5 ± 0.6	1.92 ± 0.02
60	84.3 ± 1.6	1.91 ± 0.03

administered annually were based on the dosimetry calculations (Fig. 5B). The limiting organ, based on human biodistribution data, is the kidney, which still allows for 437 MBq per year. Thus, 4 PET examinations using up to 100 MBq of ^{68}Ga-Tuna-2 are possible. ^{68}Ga-Tuna-2, thus, has a safe dosimetry profile.

DISCUSSION

^{68}Ga-Tuna-2 displays the expected biodistribution of a small peptide labeled with ^{68}Ga, exhibiting fast clearance from most tissues in combination with strong excretion-related retention in the kidney cortex. The strong retention in the kidney (especially kidney cortex) is expected to be mainly due to urinary excretion and tubular reabsorption of the radiolabeled peptide. Kidney expression of GCGR has been reported (14), and part of the renal signal may originate from receptor-mediated binding but is unlikely to be significant based on, for example, the lack of blocking effect seen in the kidneys in NHPs (6). The uptake and retention in human liver, with high density of GCGR, were elevated, in line with preclinical data in rats and NHPs.

SUV$_{55\ min}$ time point was selected as the endpoint for assessing GCGR tissue density, as the liver-to-aorta ratio was highest at this time point. PET kinetic data can sometimes be analyzed by compartmental or graphical models to increase precision. Such analysis entails estimation of an input signal, usually from the arterial curve (corrected for metabolism and plasma-to-blood ratio). However, the liver is physiologically unique in this regard as it is supplied with both arterial and venous blood, arterial blood from the hepatic artery, as well as venous blood by the portal vein. The hepatic portal vein provides the main supply, approximately 70%, of blood to the liver. Thus, kinetic modeling of PET uptake is complicated because of the need for 2 distinct input signals. Furthermore, the ratio between the venous and arterial contribution is affected by arterial stiffening, a consequence of metabolic disease. Amelioration of vascular disease by therapeutic intervention in individuals with T2D can therefore likely change the venous/arterial input signal in the liver. Because of the potential complexity
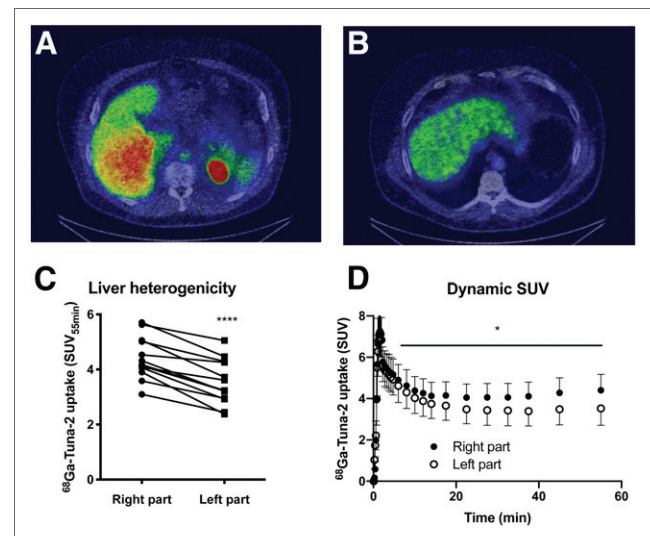
FIGURE 3. Representative transaxial images showing distinct difference in ^{68}Ga-Tuna-2 binding in right (A) and left (B) parts of liver. Images are from same time point in same individual, normalized to SUV 6 and thus directly comparable. (C) Quantitatively lower GCGR density in left part of liver was consistent in all individuals ($P < 0.001$). (D) Dynamic uptake curve in each liver part reveals that difference increased with time after injection.
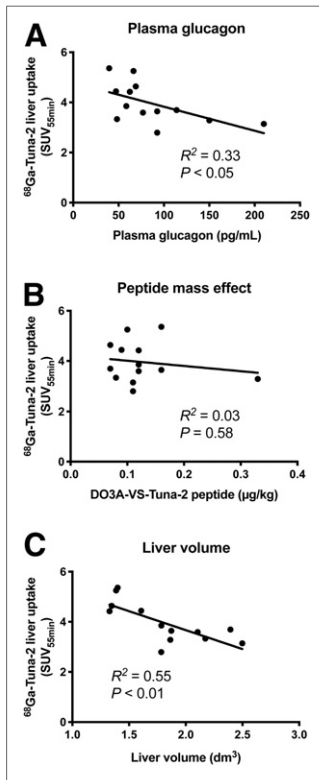
FIGURE 4. Correlations between liver binding (assessed as SUV$_{55\ min}$) of ^{68}Ga-Tuna-2 versus endogenous plasma glucagon levels (A), amount of coadministered DOTA-VS-Tuna-2 peptide (B), and liver volume (C).

in modeling the hepatic uptake, SUV was deemed as an acceptable endpoint.

The peptide mass dose of DO3A-VS-Tuna-2 in the study was estimated from dose escalation data in NHPs. From the preclinical study, it was assessed that peptide doses below 0.2 µg/kg should elicit negligible mass effect (i.e., self-blocking on the glucagon receptor, which could mask other interactions on the receptor). In the study, all subjects except 1 received the targeted dose < 0.2 µg/kg. No appreciable mass effect was seen in the subject receiving just over 0.3 µg/kg either.

As demonstrated by the sensitivity of ^{68}Ga-Tuna-2 to endogenous glucagon levels, there is a possibility that changes to the endogenous levels of glucagon interfere with the calculation of GCGR density or occupancy. Thus, it is important to ensure fasting, or to administer a standardized meal before the examination, in addition to recording the plasma glucagon levels for potential correction.

However, the conclusions drawn from the observed correlations (or their absence) are limited by the relatively small amount of examined subjects ($n = 13$), where outliers can have large impact.

An interesting and consistent feature of ^{68}Ga-Tuna-2 was the clear difference in the right and left part of the liver. The left part exhibited on average 20% lower binding in all examined individuals. Importantly, there was no difference in right and left liver part uptake during the initial perfusion phase (0–1 min), indicating that the decreased retention of ^{68}Ga-Tuna-2 in the left part represents actual lower GCGR density rather than impaired regional hepatic perfusion or tracer delivery (Fig. 3D). Furthermore, heterogeneous liver distribution of several established radiopharmaceuticals has previously been reported (15). Some exhibited up to 25% higher uptake in the left part (^{123}I-MIBG), a monoclonal antibody showed no difference between liver parts, and others demonstrated between 10% and 34% increased uptake in the right part. Because there is no consistent shift to either part reported, the implication is that there is no general difference in perfusion at basal physiology. ^{68}Ga-Tuna-2–binding patterns consequently suggest an increased GCGR density in the right part of the liver.

GCGR density in the liver as assessed by ^{68}Ga-Tuna-2 did not correlate with weight, body mass index, or age in this cohort of individuals with T2D. On the other hand, there was a negative correlation between GCGR density and liver volume ($R^2 = 0.55$, $P < 0.01$), that is, larger livers exhibited lower GCGR density (and consequently lower hepatocyte density). Liver volume, especially in T2D, may be expanded by fat content due to

nonalcoholic fatty liver disease or nonalcoholic steatohepatitis. Furthermore, high hepatic content of glycogen due to chronic increased blood glucose in turn binds up to 3–4 molar equivalents of water, thereby potentially enlarging the liver volume. An enlarged liver with unchanged amount of hepatocytes will results in an apparent decrease in hepatocyte density (and subsequently GCGR density). The negative correlation for ^{68}Ga-Tuna-2 and liver volume likely reflects these 2 processes. Any dysregulation of GCGR expression in T2D compared with nondiabetic individuals is unknown but could potentially be explored with this novel technique.

Dynamic PET distribution scanning of the entire body (several sequential whole-body passes) would be ideal for dosimetry calculations. This was not performed as it was deemed to be taxing on the enrolled individuals because they had already undergone 4 PET examinations in the full occupancy study. Thus, we have access to only the dynamic uptake in the abdominal region. However, as this region includes the critical tissues, kidney, liver, red marrow, and blood (as determined from rat and NHP distribution), we deem it suitable for dosimetry estimation (using NHP data imputation for missing, but not critical, tissues). The resulting dosimetry profile based on the human biodistribution is similar to that as predicted from NHPs. This is further evidence that ^{68}Ga-Tuna-2 can be used for repeated PET/CT scanning annually, in combination with other radiopharmaceutical agents, from a radiation safety point of view.

In summary, ^{68}Ga-Tuna-2 biodistribution in human is consistent with the known distribution of GCGR. We foresee that ^{68}Ga-Tuna-2 can be used for the assessment of liver target engagement and occupancy studies, for the emerging class of bi- or trimodal peptides targeting GCGR, in addition to, for example, GLP1R. Furthermore, this technique may improve the understanding on the role of GCGR in health in disease, for example, by assessing its variability of receptor expression in T2D compared with nondiabetic subjects.
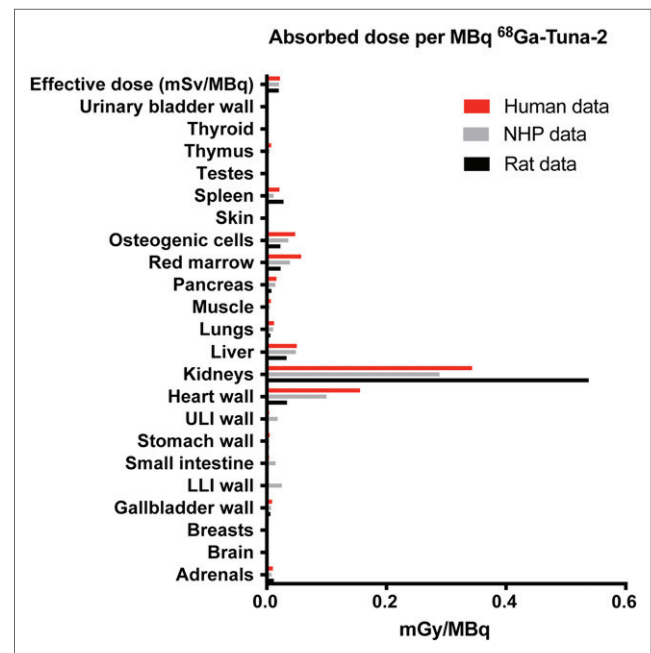
FIGURE 5. Predicted dosimetry of ^{68}Ga-Tuna-2 based on human biodistribution data, compared with previously reported NHP and rat biodistribution data. ULI = upper large intestine; LLI = lower large intestine.

Furthermore, when given intravenously at microdoses ^{68}Ga-Tuna-2 demonstrates a safe dosimetry profile and no adverse events.

CONCLUSION

[68]Ga-Tuna-2 can be used for safe and accurate assessment of the GCGR in humans. It may serve as an important tool in understanding the in vivo pharmacology of novel drugs engaging the GCGR.

DISCLOSURE

ACKNOWLEDGMENTS

KEY POINTS

QUESTION: Can ^{68}Ga-Tuna-2 PET/CT be used to image the glucagon receptor in individuals with T2D?

PERTINENT FINDINGS: In vivo imaging of hepatic glucagon receptors was feasible using ^{68}Ga-Tuna-2 PET/CT. ^{68}Ga-Tuna-2 was sensitive to endogenous levels of glucagon and exhibited a safe dosimetry profile combined with no adverse events after intravenous administration.

IMPLICATIONS FOR PATIENT CARE: ^{68}Ga-Tuna-2 can be used for safe and accurate imaging of the glucagon receptor in humans. It may serve as an important tool in understanding the role of glucagon and glucagon receptor–targeting drugs in metabolic disease.

REFERENCES

1. Müller TD, Finan B, Clemmensen C, DiMarchi RD, Tschöp MH. The new biology and pharmacology of glucagon. *Physiol Rev.* 2017;97:721–766.
2. Sánchez-Garrido MA, Brandt SJ, Clemmensen C, Müller TD, DiMarchi RD, Tschöp MH. GLP-1/glucagon receptor co-agonism for treatment of obesity. *Diabetologia.* 2017;60:1851–1861.
3. Day JW, Ottaway N, Patterson JT, et al. A new glucagon and GLP-1 co-agonist eliminates obesity in rodents. *Nat Chem Biol.* 2009;5:749–757.
4. Pocai A, Carrington PE, Adams JR, et al. Glucagon-like peptide 1/glucagon receptor dual agonism reverses obesity in mice. *Diabetes.* 2009;58:2258–2266.
5. Velikyan I, Haack T, Bossart M, et al. First-in-class positron emission tomography tracer for the glucagon receptor. *EJNMMI Res.* 2019;9:17.
6. Eriksson O, Velikyan I, Haack T, et al. A positron emission tomography biomarker for in vivo study of the glucagon receptor, assessed in non-human primates. *Sci Rep.* 2019;9:14960.
7. Evers A, Haack T, Lorenz M, et al. Design of novel exendin-based dual glucagon-like peptide 1 (GLP-1)/glucagon receptor agonists. *J Med Chem.* 2017;60: 4293–4303.
8. Elvert R, Bossart M, Herling AW, et al. Team players or opponents: coadministration of selective glucagon and GLP-1 receptor agonists in obese diabetic monkeys. *Endocrinology.* 2018;159:3105–3119.
9. Elvert R, Herling AW, Bossart M, et al. Running on mixed fuel-dual agonistic approach of GLP-1 and GCG receptors leads to beneficial impact on body weight and blood glucose control: a comparative study between mice and non-human primates. *Diabetes Obes Metab.* 2018;20:1836–1851.
10. Tillner J, Posch MG, Wagner F, et al. A novel dual glucagon-like peptide and glucagon receptor agonist SAR425899: Results of randomized, placebo-controlled first-in-human and first-in-patient trials. *Diabetes Obes Metab.* 2019;21: 120–128.
11. Eriksson O, Haack T, Hijazi Y, et al. Receptor occupancy of dual glucagon-like peptide 1/glucagon receptor agonist SAR425899 in individuals with type 2 diabetes. *Sci Rep.* 2020;10: 16758.
12. Wagner M, Doverfjord JG, Tillner J, et al. Automated GMP-compliant production of [68Ga]Ga-DO3A-Tuna-2 for PET microdosing studies of the glucagon receptor in humans. *Pharmaceuticals (Basel).* 2020;13:E176.
13. Velikyan I, Rosenstrom U, Eriksson O. Fully automated GMP production of [68Ga]Ga-DO3A-VS-Cys40-exendin-4 for clinical use. *Am J Nucl Med Mol Imaging.* 2017;7:111–125.
14. The Human Protein Atlas. GCGR. The Human Protein Atlas website. https://www.proteinatlas.org/ENSG00000215644-GCGR/tissue. Accessed February 26, 2021.
15. Jacobsson H, Jonas E, Hellström PM, Larsson SA. Different concentrations of various radiopharmaceuticals in the two main liver lobes: a preliminary study in clinical patients. *J Gastroenterol.* 2005;40:733–738.